

## Suppression of high-frequency components in off-resonant modulated driving protocols for Rydberg-blockade gates

Yuan Sun<sup>ID\*</sup>

CAS Key Laboratory of Quantum Optics and Center of Cold Atom Physics, Shanghai Institute of Optics and Fine Mechanics, Chinese Academy of Sciences, Shanghai 201800, China



(Received 9 June 2023; revised 27 July 2023; accepted 16 November 2023; published 14 December 2023)

The 2-qubit controlled-PHASE Rydberg-blockade (RB) gate via off-resonant modulated driving (ORMD) has been making significant progress recently. In pursuit of higher fidelity, faster operation, and better robustness, a major upgrade is needed with regard to suppression of high-frequency components in the modulation. A systematic method has been established here for this purpose, quintessentially to filter out the relatively higher-frequency components embedded in the basis functions that generate the modulation wave forms. Meanwhile, the 2-qubit- and multiqubit-gate conditions need to be fulfilled after filtering. It turns out that appropriate entangling-gate-protocol wave forms can be successfully obtained via this method, with the help of numerical procedures. Moreover, it can be further enhanced with adaptations to finite RB strength, as well as the dual-pulse technique to overcome residual thermal motion of qubit atoms. Besides theoretical derivations, we also thoroughly investigate the representative modulation patterns, demonstrating the versatility of ORMD in the RB gate.

DOI: 10.1103/PhysRevApplied.20.L061002

The cold-atom qubit platform [1–3] has been attracting increasing attention ever since recognition of the importance of the dipole-dipole interaction [4,5] and the successful experimental demonstration of Rydberg-blockade (RB) gates [6,7]. While the scale of qubit arrays [8–14] and single-qubit gate fidelity [15–18] are constantly advancing, enhancing the fidelity of the 2-qubit entangling gate [7,19] is one of the most pressing tasks in this field [20–22]. Recently, the advantages of the off-resonant modulated driving (ORMD) gate have been shown [23,24], where modulation in the atom-light interaction is deemed essential for this special family of controlled-PHASE (CPHASE) gates and in particular the controlled-Z (CZ) gate. It can be designed for the 1- and 2-photon ground-Rydberg transitions or even more complicated driving mechanisms [23,25], with possible extensions to ensemble qubits [26]. Along with impressive progress in the single-site addressing capability [11] and the highly coherent ground-Rydberg transition [20,21,27–30], experimental demonstrations of this category of 2-qubit gates [24,31] show clear improvement of fidelity and vast opportunities for further study.

A core feature of ORMD protocols is that the qubit-atom wave function begins and finishes at the same state, which acquires a nontrivial conditional phase shift after the time evolution. The modulation style generally consists of amplitude modulation (AM) and frequency modulation (FM) [23]. AM plays a vital role, as an analytical pulse

that starts and ends at zero intensity is usually preferable to avoid the adverse effects associated with the abrupt edges of constant-amplitude square pulses [21,25,32]. FM can be introduced as phase modulation on driving lasers or by tuning the energy of the Rydberg state via external electric, magnetic, or even microwave fields.

Given the challenge of realizing CZ-gate fidelity  $\gtrsim 0.999$  experimentally, this work aims at suppression of high-frequency (HF) components in the AM and FM wave forms, in order to upgrade the ORMD gate to the next level. It offers several advantages, both experimental and theoretical. Especially, it can avoid the distortion in the HF spectrum that occurs in electro-optical modulation instruments and help to alleviate some delicate nonadiabatic effects in the time evolution of atomic wave functions caused by the higher-order frequency components of driving fields, which may be difficult to reveal faithfully in numerical simulations. Meanwhile, it will hopefully become indispensable as part of future work on fast RB CZ gates with gate times much less than 100 ns. It may also help to maintain the quality of the dark-state driving mechanism that usually takes place in ORMD protocols. Therefore, we anticipate that the proposed method may bring about a considerable increase in the gate fidelity compared to previous approaches.

We first establish the routine of suppressing HF components of ORMD-gate wave forms in the abstract sense. Next, we demonstrate how to deploy this upgrade with 1- and 2-photon ground-Rydberg transitions. Furthermore, we work on adaptation to certain imperfections that often adversely influence experiments, including finite RB

\*yuansun@siom.ac.cn

strength and Doppler-induced dephasing caused by residual thermal motion of cold atoms. The gate fidelity here is always evaluated by the standard method [33–36].

For compatibility with numerical calculations and concise representation, a wave form  $w$  of ORMD-gate protocols can be expressed in terms of linear superposition of a complete basis  $\{g_v\}$  for  $L^2$  functions on the given finite time interval of gate operations:  $w = \sum_{v=0}^{\infty} \alpha_v g_v$ , with coefficients  $\alpha_v$ . Theoretically, it provides a tool to retrieve all possible solutions, while in practice wave forms with truncation in the expansion are sought for that can lead to high-fidelity performance. The choice of basis, such as Bernstein polynomials or Fourier series, is certainly not unique. Our major upgrade focuses on wave forms with suppressed HF components, where we assume that the HF-suppression rule is represented by an operator  $S_f$ . Suppose that  $S_f$  has the linearity property, i.e., for two wave forms  $w_1$  and  $w_2$ ,  $S_f(\alpha_1 w_1 + \alpha_2 w_2) = \alpha_1 S_f(w_1) + \alpha_2 S_f(w_2)$ ,  $\forall \alpha_1, \alpha_2 \in \mathcal{R}$ . In particular, it includes the elimination of all higher-order frequency components above a certain prescribed cutoff value. It is then straightforward to observe that  $S_f(w) = \sum_{v=0}^{\infty} S_f(g_v)$ , i.e., in principle the frequency-suppressing operation of interest is equivalent to constructing wave forms via basis functions with necessary adjustments in the frequency domain. In other words, suppression of HF components embedded in the wave form can be translated as the corresponding suppression operations on the basis functions. From the viewpoint of completeness in designing the ORMD gate, the HF suppression method introduced here is equivalent to truncation and linearly limiting coefficients in Fourier series—principles that are applicable to AM as well as FM wave forms:

$$\begin{aligned} \begin{bmatrix} v_1 \\ v_2 \\ v_3 \\ v_4 \\ v_5 \\ v_6 \end{bmatrix} &= \begin{bmatrix} 0.1273 & 0.2079 & 0.1310 & 0.0682 \\ 0.1806 & 0.1793 & 0.0282 & -0.0085 \\ 0.2242 & 0.0892 & -0.0416 & -0.0191 \\ 0.2566 & -0.0210 & -0.0386 & -0.0025 \\ 0.2766 & -0.1085 & 0.0039 & 0.0028 \\ 0.2833 & -0.1416 & 0.0272 & 0.0009 \end{bmatrix} \\ &\quad \times \begin{bmatrix} \sin \pi x \\ \sin 3\pi x \\ \sin 5\pi x \\ \sin 7\pi x \end{bmatrix}, \\ \begin{bmatrix} u_1 \\ u_2 \\ u_3 \\ u_4 \\ u_5 \end{bmatrix} &= \begin{bmatrix} 0.1710 & 0.2316 & 0.1158 \\ 0.2382 & 0.1568 & -0.0013 \\ 0.2887 & 0.0220 & -0.0408 \\ 0.3199 & -0.0986 & -0.0081 \\ 0.3305 & -0.1463 & 0.0173 \end{bmatrix} \times \begin{bmatrix} \sin \pi x \\ \sin 3\pi x \\ \sin 5\pi x \end{bmatrix}. \end{aligned} \tag{1}$$

The frequency-adjusted version of the Bernstein polynomials seems an appropriate choice for this concept. A

Bernstein polynomial  $b(x)$  is first extended as an odd function on  $[-1, 1]$  and subsequently expanded into a Fourier series. We choose  $S_f$  here to neglect all higher-order terms above a threshold. For succinctness, only two sets of frequency-adjusted functions  $\{u_j(x)\}, \{v_j(x)\}$  defined on  $x \in [0, 1]$  will be employed for symmetric wave forms. The detailed form is shown in Eq. (1), with four significant digits after the decimal point.  $u_j(x)$  corresponds to  $\hat{u}_j(x) = (b_{j,10}(x) + b_{10-j,10}(x))$  and  $v_j(x)$  corresponds to  $\hat{v}_j(x) = (b_{j,12}(x) + b_{10-j,12}(x))$ , where  $b_{v,n}(x)$  represents the  $v$ th Bernstein polynomial of degree  $n$  for  $x \in [0, 1]$ .

We denote the qubit register states as  $|0\rangle, |1\rangle$ , the Rydberg state as  $|r\rangle$ , and the singly excited Rydberg state as  $|\tilde{r}\rangle = (|r1\rangle + |1r\rangle)/\sqrt{2}$ , assuming that the qubit atoms receive homogeneous driving. There exist the 1-body process of  $|01\rangle \leftrightarrow |0r\rangle, |10\rangle \leftrightarrow |r0\rangle$  and the 2-body process of  $|11\rangle \leftrightarrow |\tilde{r}\rangle$ . Without loss of generality [37], for 1-photon transitions, the 1-body process can be described as

$$\begin{aligned} H_{s1}/\hbar &= \frac{1}{2}\Omega_1|r0\rangle\langle 10| + \frac{1}{2}\Omega_1|0r\rangle\langle 01| + \text{H.c.} \\ &\quad + \Delta_1|r0\rangle\langle r0| + \Delta_1|0r\rangle\langle 0r|, \end{aligned} \tag{2}$$

with Rabi frequency  $\Omega_1(t)$  and detuning  $\Delta_1(t)$ . Meanwhile, the 2-body process with the idealized RB effect can be described as

$$H_{s2}/\hbar = \frac{1}{\sqrt{2}}\Omega_1|\tilde{r}\rangle\langle 11| + \text{H.c.} + \Delta_1|\tilde{r}\rangle\langle \tilde{r}|. \tag{3}$$

According to the abstract principles of designing OMRD protocols, CZ-gate wave forms can be numerically computed with respect to interactions governed by  $H_{s1}$  and  $H_{s2}$ . In particular, they are first constructed via Bernstein polynomials, which then serve as the starting point of optimization procedures to acquire frequency-adjusted versions. Figure 1 shows typical results with idealized RB, where the frequency-adjusted wave forms are  $\Omega_1(x)/2\pi = 9.71u_1(x) + 13.55u_2(x) + 0.10u_3(x) + 26.29u_4(x) + 8.89u_5(x)$  MHz,  $\Delta_1(x)/2\pi = 5.358 + 5.497 \cos 2\pi x$  MHz for Fig. 1(a) and  $\Omega_1(x)/2\pi = 42.20u_1(x) - 24.93u_2(x) - 25.00u_3(x) - 42.00u_4(x) + 111.85u_5(x)$  MHz,  $\Delta_1/2\pi = 3.448$  MHz for Fig. 1(b). We use  $x = t/T_p$  and pulse time  $T_p = 250$  ns throughout. As a comparison, the original Bernstein-polynomial wave forms are  $\Omega_1(x)/2\pi = 11.58\hat{u}_1(x) + 11.28\hat{u}_2(x) + 0.03\hat{u}_3(x) + 25.65\hat{u}_4(x) + 9.57\hat{u}_5(x)$  MHz,  $\Delta_1(x)/2\pi = 4.894 + 4.927 \cos 2\pi x$  MHz for Fig. 1(a) and  $\Omega_1(x)/2\pi = 37.72\hat{u}_1(x) - 19.04\hat{u}_2(x) - 28.00\hat{u}_3(x) - 34.34\hat{u}_4(x) + 103.48\hat{u}_5(x)$  MHz,  $\Delta_1/2\pi = 3.162$  MHz for Fig. 1(b).

On the other hand, for typical 2-photon transitions [21,24,25], the 1-body process can be formulated as  $H_{d1}/\hbar = \Omega_p/2|10\rangle\langle e0| + \Omega_S/2|e0\rangle\langle r0| + \Omega_p/2|01\rangle\langle 0e| + \Omega_S/2|0e\rangle\langle 0r| + \text{H.c.} + \Delta|e0\rangle\langle e0| + \delta|r0\rangle\langle r0| + \Delta|0e\rangle\langle 0e|$

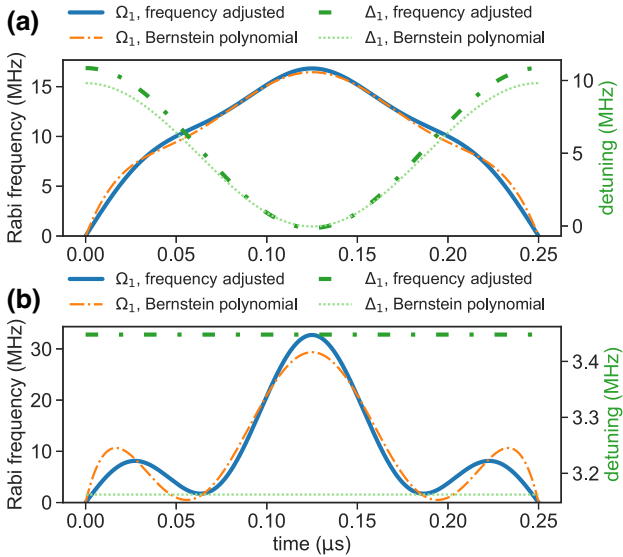


FIG. 1. CZ-gate wave forms for 1-photon transition: (a) AM and FM; (b) AM. The calculated gate errors of the frequency-adjusted wave forms are less than  $10^{-4}$ .

$\langle 0e | + \delta | 0r \rangle \langle 0r |$  with 1-photon detuning  $\Delta$  and 2-photon detuning  $\delta$ , while the 2-body process of  $|11\rangle$  with idealized RB can be formulated as  $H_{d2} = \Omega_p/\sqrt{2}|11\rangle\langle\tilde{e}| + \Omega_S/2|\tilde{e}\rangle\langle\tilde{e}| + \Omega_p/2|\tilde{r}\rangle\langle\tilde{R}| + \text{H.c.} + \Delta|\tilde{e}\rangle\langle\tilde{e}| + \delta|\tilde{r}\rangle\langle\tilde{r}| + (\Delta + \delta)|\tilde{R}\rangle\langle\tilde{R}|$ , with  $|\tilde{e}\rangle = (|e1\rangle + |1e\rangle)/\sqrt{2}$ ,  $|\tilde{R}\rangle = (|re\rangle + |er\rangle)/\sqrt{2}$ .

It turns out that HF-suppressing CZ-gate wave forms can also be successfully generated for 2-photon transitions pertinent to  $H_{d1}$  and  $H_{d2}$ , and in fact accommodating several variations of modulation style [25]. Figure 2 shows sample results: the frequency-adjusted wave forms are  $\Omega_p(x)/2\pi = 270.84u_1(x) - 25.68u_2(x) - 88.66u_3(x) - 21.08u_4(x) + 1021.0u_5(x)$  MHz,  $\delta(x)/2\pi = -0.577 + 0.101 \cos 2\pi x$  MHz for Fig. 2(a) and  $\Omega_p(x)/2\pi = 260.85u_1(x) - 11.51u_2(x) - 79.85u_3(x) + 0.0u_4(x) + 992.41u_5(x)$  MHz,  $\delta/2\pi = -0.636$  MHz for Fig. 2(b), while the wave forms on the basis of the original Bernstein polynomials are  $\Omega_p(x)/2\pi = 271.04\hat{u}_1(x) - 13.39\hat{u}_2(x) - 78.90\hat{u}_3(x) - 86.37\hat{u}_4(x) + 1073.1\hat{u}_5(x)$  MHz,  $\delta(x)/2\pi = 0.078 + 1.054 \cos 2\pi x$  MHz for Fig. 2(a) and  $\Omega_p(x)/2\pi = 193.65\hat{u}_1(x) + 85.17\hat{u}_2(x) + 0.0\hat{u}_3(x) + 291.53\hat{u}_4(x) + 649.10\hat{u}_5(x)$  MHz,  $\delta/2\pi = -0.569$  MHz for Fig. 2(b), both with  $\Omega_S/2\pi = 350$  MHz,  $\Delta/2\pi = 5000$  MHz.

Sometimes the peak power of driving lasers faces harsh practical constraints and reducing the maximum values of Rabi-frequency amplitudes becomes a priority. Fortunately, ORMD gates are capable of fulfilling this requirement without loss of fidelity or compromises of robustness and the design process can function properly with an imposed upper limit of the Rabi-frequency amplitude. Moreover, it is possible to apply the systematic method

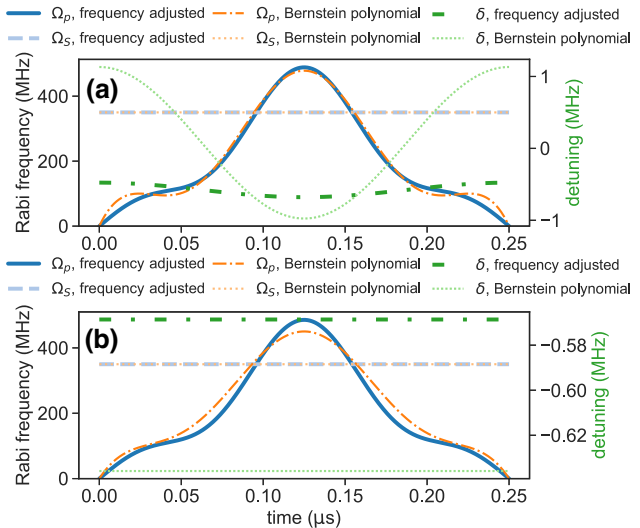


FIG. 2. CZ-gate wave forms for 2-photon transition: (a) AM and FM; (b) AM. The calculated gate errors of the frequency-adjusted version are smaller than  $10^{-4}$ .

as discussed above to suppress HF components in such wave forms. For instance, wave forms expressed by Bernstein polynomials  $b_{v,n}$  with an imposed upper limit can be approximated by linear superposition of  $b_{v,m}$  higher degree  $m > n$ , which can then be devolved to the HF suppression process. Nevertheless, as laser technology is advancing rapidly nowadays, it is worth noting that reduction of laser power is part of the more integrated strategy for better gate performance of ORMD protocols rather than a standalone requirement. The same method also applies if the FM amplitude needs restrictions.

Figure 3 presents some typical wave forms conforming to these concepts, where the frequency-adjusted versions are  $\Omega_1(x)/2\pi = 16.41v_1(x) - 0.49v_2(x) + 4.06v_3(x) + 22.38v_4(x) + 29.25v_5(x) - 2.37v_6(x)$  MHz,  $\Delta_1(x)/2\pi = 4.772 + 4.660 \cos 2\pi x$  MHz for Fig. 3(a),  $\Omega_p(x)/2\pi = 203.25v_1(x) - 5.91v_2(x) - 0.96v_3(x) + 1199.83v_4(x) + 156.87v_5(x) + 0.0v_6(x)$  MHz,  $\delta(x)/2\pi = -0.741 - 0.079 \cos 2\pi x$  MHz for Fig. 3(b), and  $\Omega_p(x)/2\pi = 200.45v_1(x) - 4.29v_2(x) + 3.14v_3(x) + 1196.44v_4(x) + 157.56v_5(x) + 0.0v_6(x)$  MHz,  $\delta/2\pi = -0.709$  MHz for Fig. 3(c) with  $\Omega_S/2\pi = 350$  MHz,  $\Delta/2\pi = 5000$  MHz. For comparison, the wave forms based on the original Bernstein polynomials with imposed limits are  $\Omega_1(x)/2\pi = \min(12.5, 23.97\hat{u}_1(x) + 0.38\hat{u}_2(x) - 4.97\hat{u}_3(x) + 25.65\hat{u}_4(x) + 38.30\hat{u}_5(x))$  MHz,  $\Delta_1(x)/2\pi = 4.427 + 5.247 \cos 2\pi x$  MHz for Fig. 3(a),  $\Omega_p(x)/2\pi = \min(350, 240.14\hat{u}_1(x) + 91.23\hat{u}_2(x) + 39.23\hat{u}_3(x) + 265.97\hat{u}_4(x) + 1360.17\hat{u}_5(x))$  MHz,  $\delta(x)/2\pi = -0.688 - 0.081 \cos 2\pi x$  MHz for Fig. 3(b), and  $\Omega_p(x)/2\pi = \min(350, 249.89\hat{u}_1(x) + 81.13\hat{u}_2(x) - 2.12\hat{u}_3(x) + 290.90\hat{u}_4(x) + 1441.72\hat{u}_5(x))$  MHz,  $\delta/2\pi = -0.661$  MHz for Fig. 3(c), also with  $\Omega_S/2\pi = 350$  MHz and  $\Delta/2\pi = 5000$  MHz.

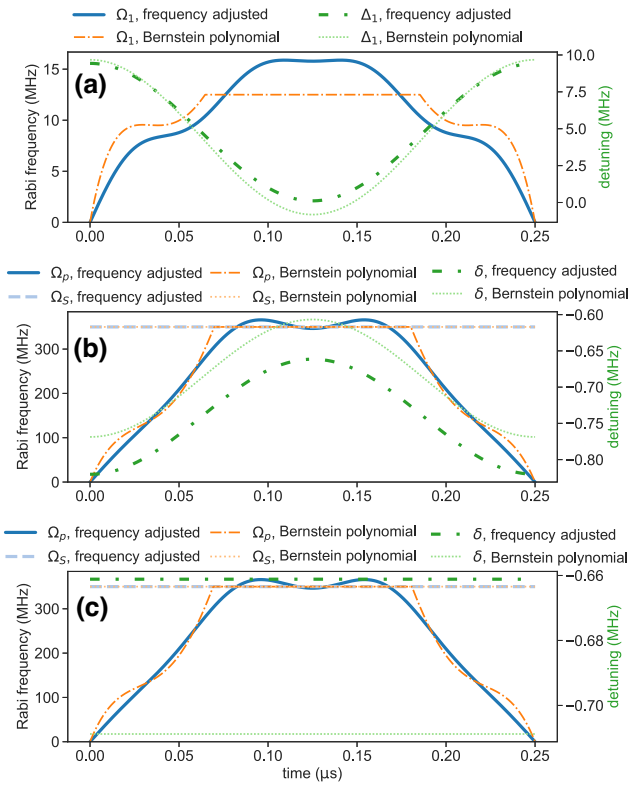


FIG. 3. CZ-gate wave forms with an imposed limit on the maximum values of Rabi-frequency amplitudes: (a) 1-photon transition; (b) 2-photon transition with both AM and FM; (c) 2-photon transition with only AM. The calculated gate errors of the frequency-adjusted version are smaller than  $10^{-4}$ .

The residual thermal motion of the qubit atoms can cause Doppler-induced dephasing [11,21] in 2-qubit gate interactions. Within the framework of ORMD-gate protocols, this type of deviation from the ideal situation usually leads to a first-order effect in phase and a second-order effect in population and if two identical pulses are applied consecutively but in completely opposite directions, their first-order effect in the phase cancels out, which brings about the dual-pulse technique [23,25]. Fortunately, HF suppression is compatible with the dual-pulse technique and hence the underlying physics does not involve any need for HF components. Figure 4 shows representative results, where the frequency-adjusted wave forms are  $\Omega_1(x)/2\pi = 8.39v_1(x) - 0.12v_2(x) - 10.0v_3(x) + 49.24v_4(x) + 29.25v_5(x) + 0.0v_6(x)$  MHz,  $\Delta_1/2\pi = 11.446$  MHz for Fig. 4(a) and  $\Omega_p(x)/2\pi = 118.41u_1(x) + 52.34u_2(x) - 99.12u_3(x) + 195.13u_4(x) + 602.87u_5(x)$  MHz,  $\delta/2\pi = -0.867$  MHz with  $\Omega_S/2\pi = 350$  MHz,  $\Delta/2\pi = 5000$  MHz for Fig. 4(b). As a comparison, the wave forms based on the original Bernstein polynomials are  $\Omega_1(x)/2\pi = \min(20, 5.90\hat{u}_1(x) - 4.61\hat{u}_2(x) + 19.58\hat{u}_3(x) + 2.36\hat{u}_4(x) + 61.84\hat{u}_5(x))$  MHz,  $\Delta_1/2\pi = 11.792$  MHz for Figure 4(a) and  $\Omega_p(x)/2\pi = 131.37\hat{u}_1(x) + 47.90\hat{u}_2(x) - 68.48\hat{u}_3(x) + 202.10\hat{u}_4(x) +$

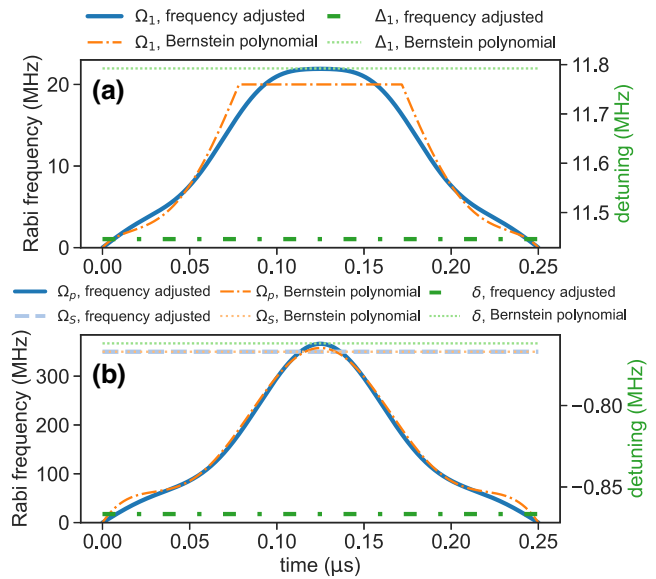


FIG. 4. CZ-gate dual-pulse technique wave forms: (a) 1-photon transition; (b) 2-photon transition. The calculated gate errors of the frequency-adjusted version are smaller than  $10^{-4}$ .

$577.29\hat{u}_5(x)$  MHz,  $\delta/2\pi = -0.762$  MHz for Figure 4(b), also with  $\Omega_S/2\pi = 350$  MHz and  $\Delta/2\pi = 5000$  MHz.

The fundamental structure of the Rydberg dipole-dipole interaction is far more complicated than the idealized RB effect [1,38–42], and ORMD with Rydberg-interaction-strength adaptation (RISA) has been devised to deal with finite RB strength [25]. According to the single-channel Förster resonance model [43] of  $|rr\rangle \leftrightarrow |qq'\rangle$  with the coupling strength as  $B$  and the small energy-penalty term as  $\delta_q$  for  $|qq'\rangle$ , the additional Hamiltonian term can be expressed by  $H_{SF} = 1/(\sqrt{2})\Omega_1|rr\rangle\langle\tilde{r}| + B|qq'\rangle\langle rr| + H.c. + 2\Delta_1(|rr\rangle\langle rr| + |qq'\rangle\langle qq'|) + \delta_q|qq'\rangle\langle qq'|$  for single-photon transition's  $H_{s2}$  and  $H_{dF} = \sqrt{2}\Omega_S/2|\tilde{R}\rangle\langle rr| + B|rr\rangle\langle qq'| + H.c. + 2\delta(|rr\rangle\langle rr| + |qq'\rangle\langle qq'|) + \delta_q|qq'\rangle\langle qq'|$  for the 2-photon transition  $H_{d2}$ . These extra complexities can be harmonically incorporated into the design process even if many more states are involved.

ORMD with RISA can perform particularly well with the frequency-adjusted versions. HF suppression produces extra benefits, possibly including a better quality of dark-state mechanism, fewer nonadiabatic effects [44,45], and less population leakage (see, e.g., Fig. 5). This helps to clarify the previously theoretically elusive point of whether a very large  $B$  is required for the RB CZ gate to reach high fidelity. For a relatively smaller value of  $B$ , non-negligible population is inevitably transferred to the 2-body doubly excited Rydberg states, which also receive a dressing on the order of  $\sqrt{B^2 + \delta_q^2}/2$ , but ORMD with RISA can take most of the moved population back via appropriate wave forms.

Following these procedures, it is certainly possible to work toward wave forms consisting of even

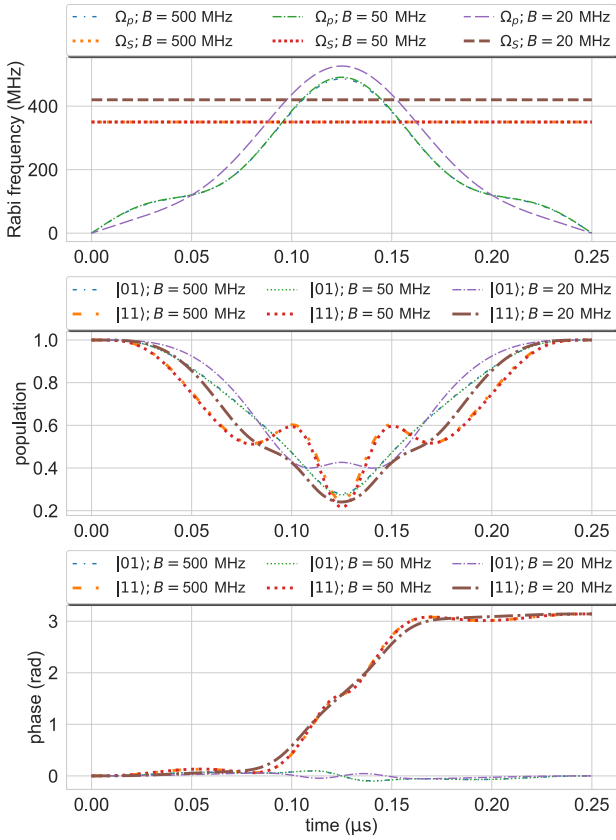


FIG. 5. Frequency-adjusted cz ORMD wave forms with RISA, with calculated gate errors  $< 10^{-4}$ .  $\delta_q = 0$  for all three cases here.

lower-frequency modulation in Rabi-frequency amplitude and detuning terms (see, e.g., Fig. 6). One may try to obtain a solution with the lowest possible frequency components in special cases but considering the finite strengths of the RB effect, suppressing scattering or leakage and many other theoretical and technical difficulties, an optimal choice does not seem to be determined by the frequency properties alone. Nevertheless, we note that unphysical numerical results with a Rabi-frequency amplitude somewhat smaller than 0 need to be neglected.

In conclusion, the design of the ORMD RB gate has been upgraded with suppression of HF components embedded in the wave forms. The results reveal that ORMD-gate protocols can function satisfactorily without the involvement of relatively higher-frequency components. A rich variety of ORMD wave forms with suppression of HF components can be derived for 1- and 2-photon ground-Rydberg transitions, including considerations for limiting peak laser intensity, the dual-pulse technique, finite RB strength, etc. This concept can also be extended to construct 2-qubit CPHASE gates with an arbitrarily designated phase and multiqubit gates, such as the 3-qubit Toffoli gate. Furthermore, it can also be helpful for other types of gate protocols or even other physical qubit

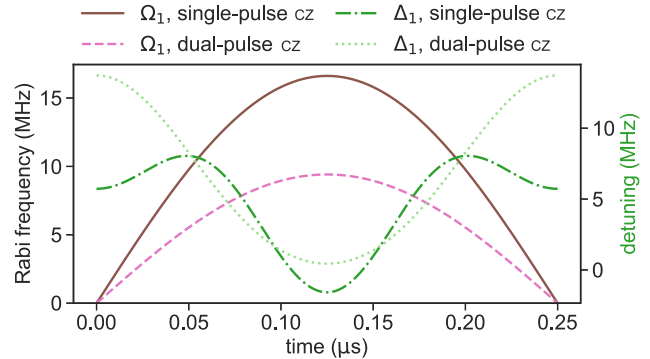


FIG. 6. Wave forms with AM of only one frequency element, the single-pulse wave form is  $\Omega_1/2\pi = 16.62 \sin \pi x$  MHz,  $\Delta_1/2\pi = 4.749 + 3.652 \cos 2\pi x - 2.677 \cos 4\pi x$  MHz and the dual-pulse wave form is  $\Omega_1/2\pi = 9.41 \sin \pi x$  MHz,  $\Delta_1/2\pi = 6.609 + 6.641 \cos 2\pi x + 0.476 \cos 4\pi x$  MHz. The calculated gate errors are smaller than  $10^{-4}$ .

platforms, including many interesting previously proposed RB-gate schemes [42,43,46–52]. This work will hopefully offer a tool for further experimental efforts in pursuit of high-fidelity and fast 2-qubit gates in the cold-atom qubit platform.

*Acknowledgments.* This work is supported by the National Natural Science Foundation of China (Grants No. 92165107 and No. 12074391) and the Chinese Academy of Sciences. I thank Ning Chen, Xiaodong He, Zhirong Lin, Peng Xu, and Hui Yan for many discussions.

- [1] M. Saffman, T. G. Walker, and K. Mølmer, Quantum information with Rydberg atoms, *Rev. Mod. Phys.* **82**, 2313 (2010).
- [2] A. Reiserer and G. Rempe, Cavity-based quantum networks with single atoms and optical photons, *Rev. Mod. Phys.* **87**, 1379 (2015).
- [3] M. Saffman, Quantum computing with atomic qubits and Rydberg interactions: Progress and challenges, *J. Phys. B: At., Mol. Opt. Phys.* **49**, 202001 (2016).
- [4] L. You and M. S. Chapman, Quantum entanglement using trapped atomic spins, *Phys. Rev. A* **62**, 052302 (2000).
- [5] D. Jaksch, *et al.*, Fast quantum gates for neutral atoms, *Phys. Rev. Lett.* **85**, 2208 (2000).
- [6] E. Urban, *et al.*, Observation of Rydberg blockade between two atoms, *Nat. Phys.* **5**, 110 (2009).
- [7] L. Isenhower, *et al.*, Demonstration of a neutral atom controlled-NOT quantum gate, *Phys. Rev. Lett.* **104**, 010503 (2010).
- [8] K. M. Maller, *et al.*, Rydberg-blockade controlled-NOT gate and entanglement in a two-dimensional array of neutral-atom qubits, *Phys. Rev. A* **92**, 022336 (2015).
- [9] Y. Wang, *et al.*, Single-qubit gates based on targeted phase shifts in a 3D neutral atom array, *Science* **352**, 1562 (2016).

- [10] D. Ohl de Mello, *et al.*, Defect-free assembly of 2D clusters of more than 100 single-atom quantum systems, *Phys. Rev. Lett.* **122**, 203601 (2019).
- [11] T. M. Graham, *et al.*, Rydberg-mediated entanglement in a two-dimensional neutral atom qubit array, *Phys. Rev. Lett.* **123**, 230501 (2019).
- [12] A. W. Young, *et al.*, Half-minute-scale atomic coherence and high relative stability in a tweezer clock, *Nature* **588**, 408 (2020).
- [13] K.-N. Schymik, *et al.*, Single atoms with 6000-second trapping lifetimes in optical-tweezer arrays at cryogenic temperatures, *Phys. Rev. Appl.* **16**, 034013 (2021).
- [14] G. Bornet, *et al.*, Scalable spin squeezing in a dipolar Rydberg atom array, *Nature* **621**, 728 (2023).
- [15] T. Xia, *et al.*, Randomized benchmarking of single-qubit gates in a 2D array of neutral-atom qubits, *Phys. Rev. Lett.* **114**, 100503 (2015).
- [16] C. Sheng, *et al.*, High-fidelity single-qubit gates on neutral atoms in a two-dimensional magic-intensity optical dipole trap array, *Phys. Rev. Lett.* **121**, 240501 (2018).
- [17] T. M. Graham *et al.*, Multi-qubit entanglement and algorithms on a neutral-atom quantum computer, *Nature* **604**, 457 (2022).
- [18] A. Jenkins, *et al.*, Ytterbium nuclear-spin qubits in an optical tweezer array, *Phys. Rev. X* **12**, 021027 (2022).
- [19] A. Gaëtan, *et al.*, Observation of collective excitation of two individual atoms in the Rydberg blockade regime, *Nat. Phys.* **5**, 115 (2009).
- [20] T. Wilk, *et al.*, Entanglement of two individual neutral atoms using Rydberg blockade, *Phys. Rev. Lett.* **104**, 010502 (2010).
- [21] Y. Liu, *et al.*, Infidelity induced by ground-Rydberg decoherence of the control qubit in a two-qubit Rydberg-blockade gate, *Phys. Rev. Appl.* **15**, 054020 (2021).
- [22] G. D. Kahanamoku-Meyer, *et al.*, Classically verifiable quantum advantage from a computational Bell test, *Nat. Phys.* **18**, 918 (2022).
- [23] Y. Sun, *et al.*, Controlled phase gate protocol for neutral atoms via off-resonant modulated driving, *Phys. Rev. Appl.* **13**, 024059 (2020).
- [24] Z. Fu, *et al.*, High-fidelity entanglement of neutral atoms via a Rydberg-mediated single-modulated-pulse controlled-phase gate, *Phys. Rev. A* **105**, 042430 (2022).
- [25] Y. Sun, Off-resonant modulated driving gate protocols for two-photon ground-Rydberg transition and finite Rydberg blockade strength, *Opt. Express* **31**, 3114 (2023).
- [26] M. Ebert, *et al.*, Coherence and Rydberg blockade of atomic ensemble qubits, *Phys. Rev. Lett.* **115**, 093601 (2015).
- [27] Y.-Y. Jau, *et al.*, Entangling atomic spins with a Rydberg-dressed spin-flip blockade, *Nat. Phys.* **12**, 71 (2015).
- [28] K. McDonnell, L. F. Keary, and J. D. Pritchard, Demonstration of a quantum gate using electromagnetically induced transparency, *Phys. Rev. Lett.* **129**, 200501 (2022).
- [29] Y. Chew, *et al.*, Ultrafast energy exchange between two single Rydberg atoms on a nanosecond timescale, *Nat. Photonics* **16**, 724 (2022).
- [30] Y.-X. Chao, *et al.*, Pound-Drever-Hall feedforward: Laser phase noise suppression beyond feedback, *arXiv:2309.09759*.
- [31] S. J. Evered, *et al.*, High-fidelity parallel entangling gates on a neutral-atom quantum computer, *Nature* **622**, 268 (2023).
- [32] S. Jandura and G. Pupillo, Time-optimal two- and three-qubit gates for Rydberg atoms, *Quantum* **6**, 712 (2022).
- [33] A. Jamiołkowski, Linear transformations which preserve trace and positive semidefiniteness of operators, *Rep. Math. Phys.* **3**, 275 (1972).
- [34] M.-D. Choi, Completely positive linear maps on complex matrices, *Linear Algebra Appl.* **10**, 285 (1975).
- [35] A. Gilchrist, N. K. Langford, and M. A. Nielsen, Distance measures to compare real and ideal quantum processes, *Phys. Rev. A* **71**, 062310 (2005).
- [36] L. H. Pedersen, N. M. Møller, and K. Mølmer, Fidelity of quantum operations, *Phys. Lett. A* **367**, 47 (2007).
- [37] See supplemental material at <http://link.aps.org-supplemental/10.1103/PhysRevApplied.20.L061002> for more details and more examples of suppressing high-frequency components in ORMD.
- [38] K. Singer, *et al.*, Long-range interactions between alkali Rydberg atom pairs correlated to the ns-ns, np-np and nd-nd asymptotes, *J. Phys. B: At., Mol. Opt. Phys.* **38**, S295 (2005).
- [39] D. Cano and J. Fortágh, Multiatom entanglement in cold Rydberg mixtures, *Phys. Rev. A* **89**, 043413 (2014).
- [40] Y. Zeng, *et al.*, Entangling two individual atoms of different isotopes via Rydberg blockade, *Phys. Rev. Lett.* **119**, 160502 (2017).
- [41] R.-H. Zheng, *et al.*, Robust and high-fidelity nondestructive Rydberg parity meter, *Phys. Rev. A* **102**, 012609 (2020).
- [42] J.-L. Wu, *et al.*, Resilient quantum gates on periodically driven Rydberg atoms, *Phys. Rev. A* **103**, 012601 (2021).
- [43] D. Petrosyan, *et al.*, High-fidelity Rydberg quantum gate via a two-atom dark state, *Phys. Rev. A* **96**, 042306 (2017).
- [44] F. Motzoi, *et al.*, Simple pulses for elimination of leakage in weakly nonlinear qubits, *Phys. Rev. Lett.* **103**, 110501 (2009).
- [45] Y. Sun and H. Metcalf, Nonadiabaticity in stimulated Raman adiabatic passage, *Phys. Rev. A* **90**, 033408 (2014).
- [46] D. D. B. Rao and K. Mølmer, Robust Rydberg-interaction gates with adiabatic passage, *Phys. Rev. A* **89**, 030301 (2014).
- [47] M. Saffman, *et al.*, Symmetric Rydberg controlled-Z gates with adiabatic pulses, *Phys. Rev. A* **101**, 062309 (2020).
- [48] J. T. Young, *et al.*, Asymmetric blockade and multiqubit gates via dipole-dipole interactions, *Phys. Rev. Lett.* **127**, 120501 (2021).
- [49] J.-L. Wu, *et al.*, Systematic-error-tolerant multiqubit holonomic entangling gates, *Phys. Rev. Appl.* **16**, 064031 (2021).
- [50] R. Li, *et al.*, Optimal model for fewer-qubit CNOT gates with Rydberg atoms, *Phys. Rev. Appl.* **17**, 024014 (2022).
- [51] S.-L. Su, *et al.*, Rabi- and blockade-error-resilient all-geometric Rydberg quantum gates, *Phys. Rev. Appl.* **19**, 044007 (2023).
- [52] R. Li, J. Qian, and W. Zhang, Proposal for practical Rydberg quantum gates using a native two-photon excitation, *Quantum Science and Technology* **8**, 035032 (2023).